

Integrated on-chip inductors with electroplated magnetic yokes (invited)

Naigang Wang, Eugene J. O'Sullivan, Philipp Herget, Bipin Rajendran, Leslie E. Krupp et al.

Citation: *J. Appl. Phys.* **111**, 07E732 (2012); doi: 10.1063/1.3679458

View online: <http://dx.doi.org/10.1063/1.3679458>

View Table of Contents: <http://jap.aip.org/resource/1/JAPIAU/v111/i7>

Published by the [American Institute of Physics](#).

Related Articles

Single-core fluxgate gradiometer with simultaneous gradient and homogeneous feedback operation

J. Appl. Phys. **111**, 07E328 (2012)

A single-solenoid pulsed-magnet system for single-crystal scattering studies

Rev. Sci. Instrum. **83**, 035101 (2012)

Solution to the problem of E-cored coil above a layered half-space using the method of truncated region eigenfunction expansion

J. Appl. Phys. **111**, 07E717 (2012)

Array of 12 coils to measure the position, alignment, and sensitivity of magnetic sensors over temperature

J. Appl. Phys. **111**, 07E501 (2012)

Skin effect suppression for Cu/CoZrNb multilayered inductor

J. Appl. Phys. **111**, 07A501 (2012)

Additional information on *J. Appl. Phys.*

Journal Homepage: <http://jap.aip.org/>

Journal Information: http://jap.aip.org/about/about_the_journal

Top downloads: http://jap.aip.org/features/most_downloaded

Information for Authors: <http://jap.aip.org/authors>

ADVERTISEMENT



FIND THE NEEDLE IN THE HIRING HAYSTACK

Post jobs and reach
thousands of hard-to-find
scientists with specific skills



<http://careers.physicstoday.org/post.cfm> **physicstoday JOBS**

Integrated on-chip inductors with electroplated magnetic yokes (invited)

Naigang Wang,^{1,a)} Eugene J. O'Sullivan,¹ Philipp Herget,² Bipin Rajendran,¹ Leslie E. Krupp,² Lubomyr T. Romankiw,¹ Bucknell C. Webb,¹ Robert Fontana,² Elizabeth A. Duch,¹ Eric A. Joseph,¹ Stephen L. Brown,¹ Xiaolin Hu,³ Gary M. Decad,² Noah Sturcken,⁴ Kenneth L. Shepard,⁴ and William J. Gallagher¹

¹IBM Research Division, Thomas J. Watson Research Center, P.O. Box 218, Yorktown Heights, New York 10598, USA

²IBM Research Division, Almaden Research Center, 650 Harry Road, San Jose, California 95120, USA

³Mt. Holyoke College, 50 College Street, South Hadley, Massachusetts 01075, USA

⁴Department of Electrical Engineering, Columbia University, New York, New York 10027, USA

(Presented 2 November 2011; received 5 October 2011; accepted 13 December 2011; published online 13 March 2012)

Thin-film ferromagnetic inductors show great potential as the energy storage element for integrated circuits containing on-chip power management. In order to achieve the high energy storage required for power management, on-chip inductors require relatively thick magnetic yoke materials (several microns or more), which can be readily deposited by electroplating through a photoresist mask as demonstrated in this paper, the yoke material of choice being Ni₄₅Fe₅₅, whose properties of relatively high moment and electrical resistivity make it an attractive model yoke material for inductors. Inductors were designed with a variety of yoke geometries, and included both single-turn and multi-turn coil designs, which were fabricated on 200 mm silicon wafers in a CMOS back-end-of-line (BEOL) facility. Each inductor consisted of electroplated copper coils enclosed by the electroplated Ni₄₅Fe₅₅ yokes; aspects of the fabrication of the inductors are discussed. Magnetic properties of the electroplated yoke materials are described, including high frequency permeability measurements. The inductance of 2-turn coil inductors, for example, was enhanced up to about 6 times over the air core equivalent, with an inductance density of 130 nH/mm² being achieved. The resistance of these non-laminated inductors was relatively large at high frequency due to magnetic and eddy current losses but is expected to improve as the yoke material/structure is further optimized, making electroplated yoke-containing inductors attractive for dc-dc power converters. © 2012 American Institute of Physics. [doi:10.1063/1.3679458]

I. INTRODUCTION

The use of on-chip power converters to minimize distribution losses and achieve fast transient response is an attractive approach to realizing highly granular power management for modern microprocessors.^{1–3} Inductors are one of the key passive elements for dc-dc power converters. The air-core inductors that are widely used in RF-integrated circuits usually have low inductance (<10 nH). Therefore, high-performance, soft-magnetic-material yokes have to be added to the inductors to improve the energy storage. Such high performance inductors are still largely unavailable, especially in the on-chip format most desirable for high efficiency, which hinders the development of on-chip power converters.

On-chip inductors bring about a new set of challenges and opportunities not found in their discrete board-level counterparts. Their small size forces the use of a higher frequency converter and the adoption of materials that will operate at these frequencies. Their dimensional constraints compel the use of thin film deposition techniques, which may restrict the types of materials that can be used. Micro-magnetic properties, such as magnetic anisotropy and domain structure, have to be precisely controlled to achieve

good magnetic performance. Most importantly, fabrication challenges have to be solved, such as alignment/overlay and patterning, and overcoming the effects of film stress in, and poor adhesion of, relatively thick films. Thanks to the recent development of spin electronics, magnetic materials are becoming accepted by semiconductor industries, which is timely for developing magnetic inductors. In addition, the thin film recording head industry has accumulated a wealth of knowledge and experience relating to the deposition of soft magnetic materials and head fabrication, much of which can be borrowed for building on-chip inductors.

The figures of merit for the soft magnetic materials used for on-chip inductors are high moment, low coercivity, high anisotropy, and high electrical resistivity. These properties are chosen to reduce magnetic hysteresis and eddy current losses, while maintaining the ability to handle high currents and store high energy. Additionally, a low-cost fabrication method that is compatible with CMOS processing is desirable for the production of on-chip inductors, especially since 200 mm CMOS back-end-of-line (BEOL) facilities used by the silicon industry could be adapted for inductor fabrication. In order to achieve the high energy storage required for power management, on-chip inductors tend to require relatively thick magnetic yoke materials (e.g., a few microns). The deposition of magnetic films such as Co-Ta-Zr, Ni₂₀Fe₈₀ and Fe-N using vacuum deposition techniques has been

^{a)}Author to whom correspondence should be addressed. Electronic mail: nwang@us.ibm.com.

described by.⁴⁻⁶ Vacuum methods have the ability to deposit a large variety of magnetic materials and to easily produce laminated structures. However, they usually have low deposition rates, they may not have good conformal coverage,⁵ and the derived magnetic films may be difficult to pattern (e.g., due to pattern alignment reasons and long etching times). Electroplating is a powerful technique for the deposition of thick metal films due to its high deposition rate, conformal coverage, ability to plate through a mask, and low cost, making it a good candidate for the fabrication of magnetic yokes.

In this paper, thin-film on-chip inductors with electroplated $\text{Ni}_{45}\text{Fe}_{55}$ magnetic yokes will be introduced. Figure 1 shows a schematic of the inductors, which have an elongated spiral topology. Similar structures have been reported to show high inductance density and quality factor at relatively high frequencies.⁴ The inductors were designed with a variety of yoke geometries and included both single-turn and multi-turn coil designs. Each magnetic inductor contained an electroplated copper coil enclosed by the electroplated $\text{Ni}_{45}\text{Fe}_{55}$ yokes; air-core inductors were also fabricated. The $\text{Ni}_{45}\text{Fe}_{55}$ material was chosen for its relatively high magnetic moment, high anisotropy field, and relatively high electrical resistivity; it was first introduced into thin film heads by IBM in 1997,⁷ and it was also recently employed in on-chip inductors.^{8,9} Measurements of the magnetic properties of the electroplated yoke materials will be described, including high frequency permeability measurements. Aspects of the design and fabrication of the inductors will be discussed. Finally, the performance of various fabricated inductors will be described.

II. FABRICATION

The inductors were fabricated on 200 mm silicon wafers in the Materials Research Laboratory (MRL) at the T.J. Watson Research Center. The bottom and top inductor yokes were electroplated galvanostatically in a paddle cell. The details of the bath composition and the plating process were described in Ref. 10. In contrast to Refs. 8 and 9, which claimed that pulse plating is essential to achieve the desired plating thickness and compositional uniformity, simple dc plating was found to work well by employing judicious device design; a deposition rate of 160 nm/min was obtained. Physical vapor deposited

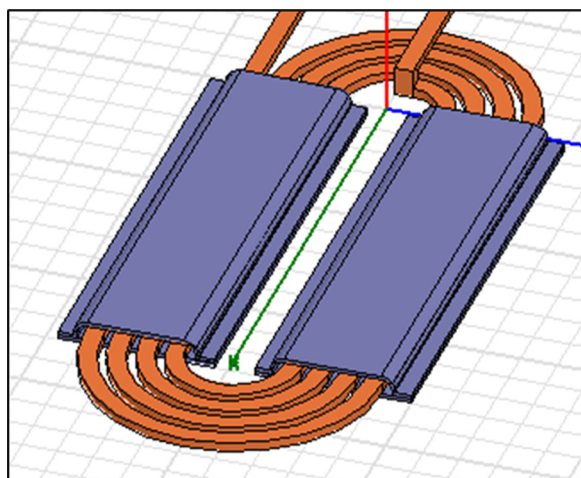


FIG. 1. (Color online) Schematic of the on-chip inductors.

(PVD) $\text{Ni}_{80}\text{Fe}_{20}$ films, 65 nm thick, were used as the electroplating seedlayers; a bias magnetic field was applied during seedlayer deposition to produce magnetic anisotropy. The magnetic yokes were plated through photoresist-defined molds (thru-mask plating method). This method gave smooth yoke edges, edge smoothness being important to avoid the nucleation of magnetic domains and pinning of domain walls. To ensure good yoke deposit thickness and composition uniformity, the field around the yokes was also plated up at the same time as the yokes, a thin resist frame separating both plated regions. During plating, a dc magnetic field was applied along the longest yoke axis to define the magnetic anisotropy of the yokes. The presence of the field material ensures continuous magnetic flux across the whole 200 mm wafer, which is critical for obtaining good magnetic anisotropy.

After yoke plating, resist mask stripping, and plated field and seedlayer etching, a bilayer of PECVD SiN_x and TEOS dielectric (which were a little more than 1 μm in total thickness) was used to encapsulate the yokes. After bottom yoke fabrication, the magnetic vias, where the top and bottom yokes contact, were opened by reactive ion etching (RIE). Following plating seedlayer deposition, copper coils were electroplated through resist masks to a thickness of about 5 μm . After resist mask and seedlayer removal, 6 μm -thick photoresist (AZ Electronics P4620) was used to encapsulate the coils. After patterning, the photoresist was briefly reflowed at 120 $^{\circ}\text{C}$ to give sloped sidewalls, ensuring that the top yokes gradually extended to the magnetic via, avoiding forming an abrupt angle, which could saturate or pin domain walls. Finally, the photoresist was hard-baked at ca. 200 $^{\circ}\text{C}$ for 2 h to form a rigid encapsulant. The hard-baked photoresist structures exhibited smooth and partially planar surfaces in advance of top yoke plating.

After top yoke fabrication and encapsulation by a bilayer of PECVD SiN_x and TEOS, inductor fabrication was concluded by opening the electrical contacts (Cu pads) using RIE. Figure 2 shows cross-sections of a single-turn inductor and a magnetic via, while Fig. 3 shows pictures of typical inductors. It can be seen that the yokes are uniform in thickness across the whole device, including the sloped hard-baked resist regions near the vias.

III. MAGNETIC MATERIALS PROPERTIES

The resistivity of the electroplated $\text{Ni}_{45}\text{Fe}_{55}$ was measured to be ca. 45 $\mu\Omega\cdot\text{cm}$ using the four-point probe method, which is double the resistivity of Permalloy ($\text{Ni}_{81}\text{Fe}_{19}$). The higher resistivity of the former material should help to reduce eddy current at high frequency. The stress of $\text{Ni}_{45}\text{Fe}_{55}$ films was determined by measuring the curvature change of a silicon wafer before and after film plating; a relatively low tensile stress of 132 MPa for 1.0 μm -thick films was observed. Nevertheless, the relatively high magnetostriction of $\text{Ni}_{45}\text{Fe}_{55}$ could degrade magnetic properties even in the case of electrodeposits with low internal stress.⁷

Figure 4 shows the magnetic hysteresis loops, which were obtained using a VSM (MicroSense model 10), of a plated $\text{Ni}_{45}\text{Fe}_{55}$ film with a thickness of 2.0 μm ; the area of the sample was 1 cm^2 . The film shows clear anisotropy with a low coercivity of 0.2 Oe along both easy and hard axes.

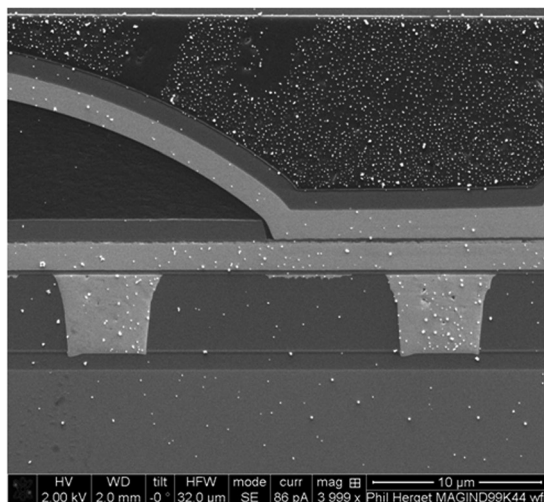
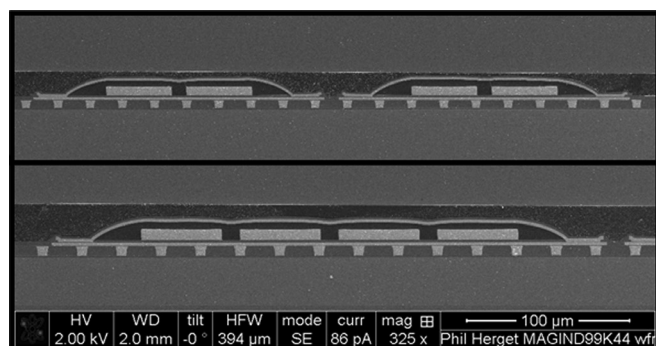


FIG. 2. SEM cross-sections of magnetic inductors.

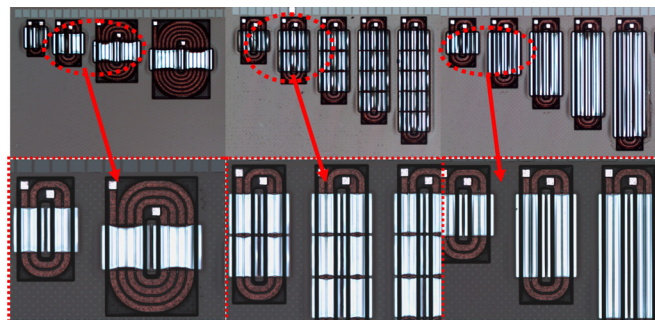
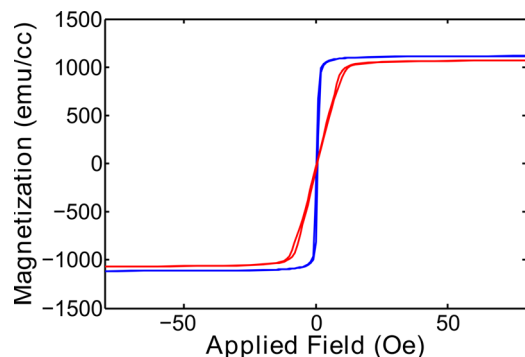


FIG. 3. (Color online) Pictures of typical fabricated magnetic inductors.

FIG. 4. (Color online) Hysteresis loop of a plated $\text{Ni}_{45}\text{Fe}_{55}$ film.TABLE I. Summary of the properties of electroplated $\text{Ni}_{45}\text{Fe}_{55}$ films.

Property	$\text{Ni}_{45}\text{Fe}_{55}$
Bs (T)	1.5 T
H_k (Oe)	13
H_c (Oe)	0.2 (Easy)
	0.2 (Hard)
Resistivity ($\mu\Omega\cdot\text{cm}$)	45
Density (kg/m^3)	$\sim 8.3 \times 10^3$
Stress as plated (MPa)	132 (1 μm)
	114 (2.5 μm)
	97 (3 μm)

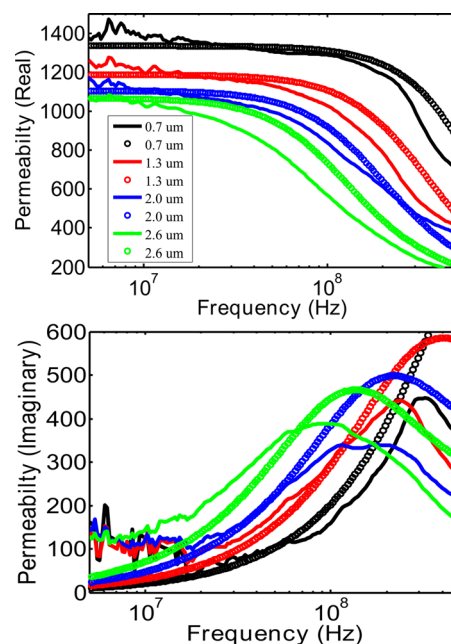
Saturation magnetization and anisotropy fields are 1.5 T and 13 Oe, respectively. Table I summarizes the properties of the $\text{Ni}_{45}\text{Fe}_{55}$ material.

Complex permeability spectra were obtained by measuring the impedance of a single-stripe loop fixture loaded with magnetic films.¹¹ Figure 5 shows the real and complex permeability spectra of plated $\text{Ni}_{45}\text{Fe}_{55}$ films with different thicknesses for a frequency range of 5 MHz to 500 MHz. For comparison, theoretical permeability spectra are also shown in the circle lines. Taking into account the eddy current, the theoretical permeability may be calculated by the following equation¹²

$$\mu_r = \mu' + \mu'' = \mu_{ri} \frac{(1-i)e^{(1+i)d/\delta} - 1}{d/\delta} \frac{e^{(1+i)d/\delta} - 1}{e^{(1+i)d/\delta} - 1}, \quad (1)$$

where d is the thickness of the film, δ is the skin depth, and μ_{ri} is derived from Landau-Lifshitz-Gilbert (LLG) equation considering only the coherent magnetization rotation

$$\mu_i = \left(\frac{\gamma M_s}{\gamma H_k + i\alpha\omega} \right) \times \left[1 + \frac{\omega^2}{(\gamma H_k + \gamma M_s + i\alpha\omega)(\gamma H_k + i\alpha\omega) - \omega^2} \right] + 1. \quad (2)$$

FIG. 5. (Color online) Complex permeability spectra of $\text{Ni}_{45}\text{Fe}_{55}$ films with different thicknesses. For comparison, theoretical permeability spectra are also shown in the circle lines.

In Eq. (2), M_s is the saturation magnetization, H_k is the anisotropy field, γ is the gyromagnetic ratio, and α is the damping constant.¹³ The measured data are in good agreement with the calculated results. The low frequency permeability reached a value of 1300 for the $0.7\ \mu\text{m}$ films. As the thickness of the film increased, the value decreased to about 1000 for the $2.6\ \mu\text{m}$ film due to the shape anisotropy induced in the thicker films. In addition, due to eddy current and skin effects, the roll-off frequency decreased from 200 MHz to 50 MHz as the thickness increased.

The achievement of proper domain structures is critical for well-behaved magnetic behavior. Coherent rotation is preferred to domain wall motion due to its faster response and lower loss. In addition, the presence of closure domains at yoke edges can degrade magnetic performance. Figure 6 shows the domain structures of electroplated bottom yokes. The magnetic domain image was obtained by decorating domain walls using ferrofluid (FerroTech EMG508). The long strip domains indicate a uniaxial anisotropy. Closure domains were observed at the ends of the yokes in addition to large spike domains. These closure domains play an important role in the inductor performance, as will be shown later.

IV. INDUCTOR PERFORMANCE

The dc resistances of the inductors on a whole (200 mm) wafer were screened by an automatic 4-point probe system. Figure 7 shows a histogram of the dc resistance distribution for a 1 mm-long, 2-turn inductor for all 45 chips on the 200 mm wafer; dc resistances were $0.158\ \Omega$, with a standard deviation of $0.057\ \Omega$.

The small-signal impedances of the inductors were measured as a function of frequency using an Agilent 8753ES network analyzer with GGB Industries ground-signal microwave probes. Figure 8 shows the inductance data for 2-turn-coil inductors with yoke thicknesses of $1.0\ \mu\text{m}$ and $1.5\ \mu\text{m}$, respectively, both inductors having the same yoke length of 1.25 mm. For comparison, the data for air-core inductors with identical coils is also shown. By introducing magnetic materials, it can be seen that the low frequency inductances were enhanced by $4\times$ and $6\times$ for the $1.0\ \mu\text{m}$ and $1.5\ \mu\text{m}$ yoke thicknesses, respectively. The inductance is proportional to the yoke thickness, as predicted in the model¹⁴ given by

$$L = \mu_0 \mu_r \frac{t}{2} \frac{l}{w}, \quad (3)$$

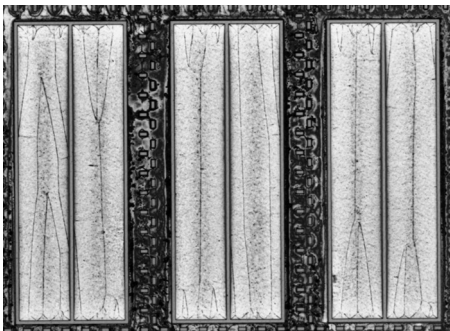


FIG. 6. Magnetic domain structure of electroplated bottom yokes.

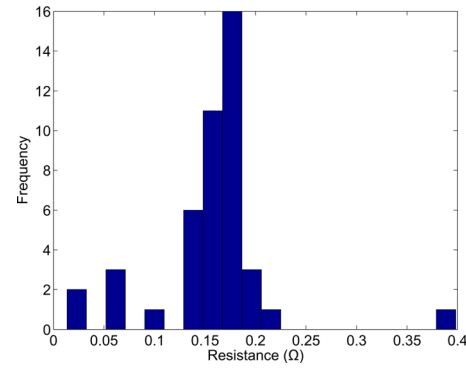


FIG. 7. (Color online) Histogram of dc resistances measured for a 1 mm-long, 2-turn type inductor for all chips on a 200 mm wafer.

where t , l , and w are the thickness, length, and width of the yoke, respectively.

As the frequency increased from 10 to 20 MHz, the inductance of the inductors with thicker yokes began to roll-off due to increasing eddy current and skin effects. The rapid increase in eddy current loss resulted in a quality factor maximum of 3 being observed only (Fig. 8). Compared to the permeability spectrum of the thin films in Fig. 5, the onset of roll-off occurred at much lower frequency in the case of the inductors, which suggests differences in $\text{Ni}_{45}\text{Fe}_{55}$ properties when in yoke form. These changes are potentially caused by shape and stress effects, and possibly also by the fabrication

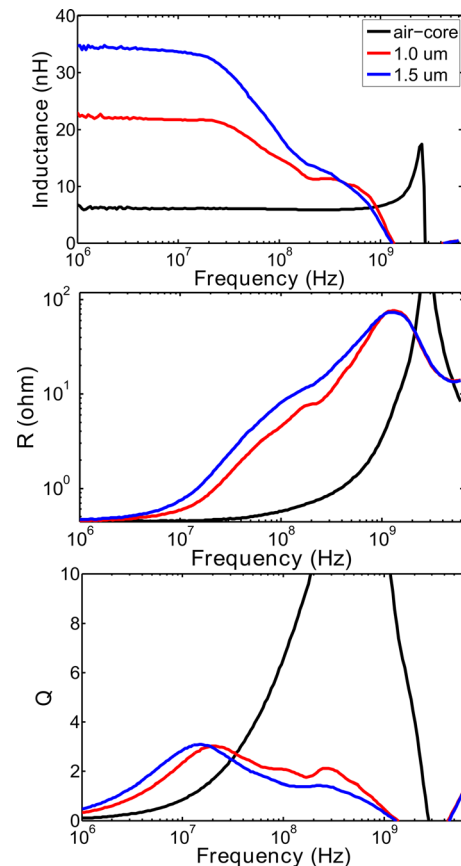


FIG. 8. (Color online) Measurements of 2-turn-coil inductors with yoke thickness of $1.0\ \mu\text{m}$ and $1.5\ \mu\text{m}$, respectively. For comparison, the measurement data of air-core inductors with identical coils are also shown.

conditions. The inductance continued rolling off as the frequency increased, the rate of inductance decrease slowing down before the onset of the self-resonant region; finally, the inductance rapidly decreased to zero.

Both the inductance density (130 nH/mm^2) and quality factor (3) are lower than the maximum values (1700 nH/mm^2 and $Q = 7$) reported for similar on-chip inductors with physical vapor deposited magnetic materials, such as Co-Zr-Ta.^{4,15} This difference in performance may be due not only to the relatively low resistivity of $\text{Ni}_{45}\text{Fe}_{55}$ (giving a low Q value), but also to the effects of magnetostriction in the $\text{Ni}_{45}\text{Fe}_{55}$ material, which may significantly lower the effective device permeability, and thus the inductance density.

Figures 9(a) and 9(b) show the performance of 2-turn inductors with different yoke lengths, whose yoke thicknesses are 1.0 and $1.5 \mu\text{m}$, respectively. For both sets of inductors, the inductors with shortest yoke lengths ($250 \mu\text{m}$) showed marginal enhancement of inductance, and, thus, they behaved like air core inductors. This may be caused by the close proximity of the domains formed at the ends of the yokes. These closure domains will not be responsive to excitation when the inductors operate at low currents; hence no obvious inductance improvements were observed. The inductors with longer yokes, on the other hand, all had inductance larger than that of air core inductors, and the low frequency inductance increased linearly with yoke length, which is also consistent with the model described in Eq. (3).

Figure 10 shows the measured data for inductors with different numbers of coil turns. The yokes in these inductors are $1.5 \mu\text{m}$ thick and 1 mm long, and contain a coil of width $40 \mu\text{m}$. The low frequency inductance of the 6-turn inductor reached a value of 125 nH . In addition, as the number of coil turns increased, the self-resonant frequencies of the inductors decreased from 40 GHz to 200 MHz . This may be caused by the increased capacitances associated with the Cu coils, for

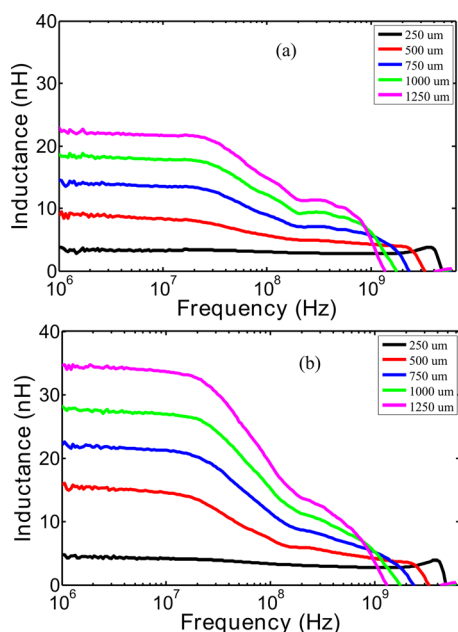


FIG. 9. (Color online) Measurements of the inductors with different yoke lengths. The yoke thickness is (a) $1.0 \mu\text{m}$ and (b) $1.5 \mu\text{m}$.

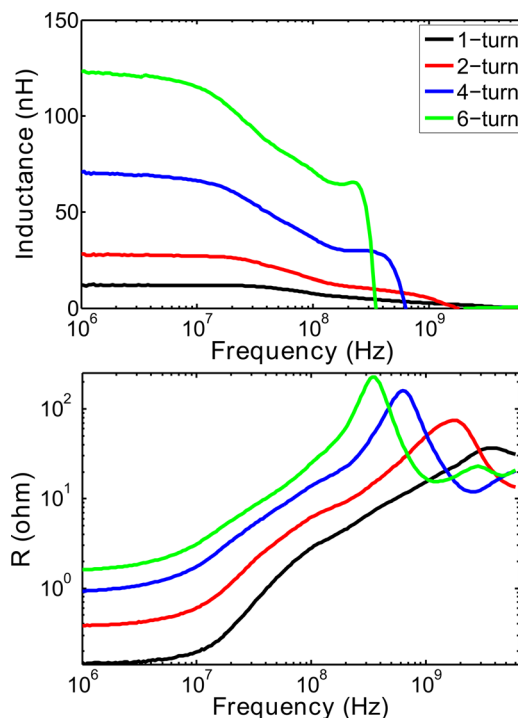


FIG. 10. (Color online) Measurements of inductors with different number turns of coils.

example, the capacitance between the turns of the coils, between coils and substrate, and between the coils and yokes. A complete model is required to calculate the total capacitance, which will not be discussed here.

Air gaps are often introduced into magnetic circuits in order to store more energy, control inductance, and to

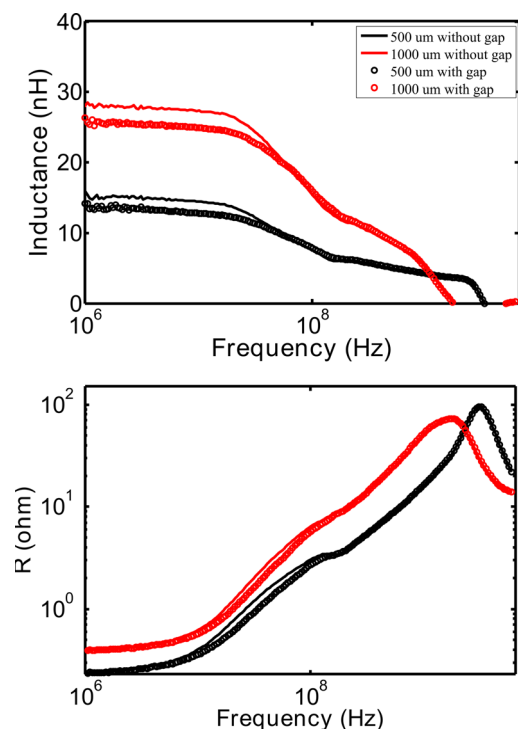


FIG. 11. (Color online) Measurements of inductors with and without gaps at magnetic via.

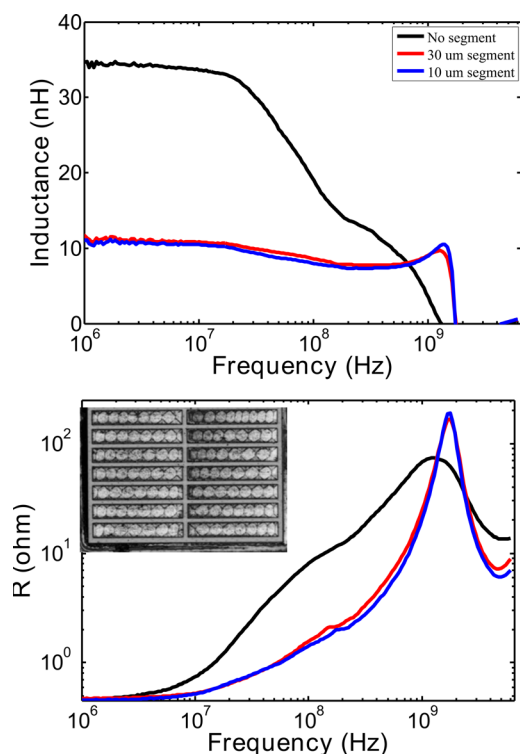


FIG. 12. (Color online) Measurements of the inductors with segmented yokes.

prevent the magnetic materials from saturating.¹⁶ Figure 11 shows results for inductors with and without gaps at the magnetic via. The gaps, which are filled with TEOS plus a thin layer of SiN_x as described earlier, have a thickness of ca. 1.2 μm . Two 2-turn inductors were studied, which had yoke lengths of 500 and 1000 μm , respectively. By introducing the gaps, the low frequency inductance decreased only about 7% due to the low reluctance of the air gap (large area and short length); however, at high frequency, the inductors with air gaps exhibited lower resistance, which lead to higher roll-off frequencies and larger quality factors.

One way to control eddy current in the magnetic materials is to pattern transverse slots into the yokes.¹⁷ Figure 12 shows the behavior of 2-turn inductors with such segmented yokes. The inductors had the same coil size, yoke thickness, and total yoke length. The slots had the same width of 10 μm , but the number of slots per yoke varied so that the width of each magnetic segment was 30 μm in the case of one yoke, and 10 μm in the case of the other. Unlike those described in Ref. 6, the slots were introduced at the same location in both bottom and top yokes so that each yoke segment completely enclosed the coils. The results indicate that both segmented devices behaved similarly to each other, but were significantly different from the inductors without segmented yokes. Similar to the inductors with short yokes, the inductors with segmented yokes showed no obvious

enhancement of the inductance compared with air core inductors. The slots changed the shape anisotropy of each segment, so that the easy-axis defined during plating was forced to be perpendicular to the long axis of the segment. Therefore, closure magnetic domain structures were easily formed in the segment structure as shown in the picture (inset of Fig. 12). These closure domains will not respond to small signal input power, and, thus, only a small enhancement of the inductance was measured.

V. CONCLUSION

Fabrication of on-chip magnetic inductors on 200 mm wafers has been demonstrated. Electroplating through a resist mask was used to produce the Ni₄₅Fe₅₅ magnetic yoke materials with good control of film thickness, composition, and magnetic properties. By incorporating magnetic materials, the inductance of 2-turn coil inductors was enhanced up to about 6 times over the air core equivalent; an inductance density of 130 nH/mm² was obtained. The resistance of the inductors was relatively large at high frequency due to magnetic and eddy current losses; improved inductor performance is expected through yoke lamination and/or adoption of more resistive yoke material. With further optimization, thin-film inductors with electroplated yokes are expected to show increasing promise for use in integrated on-chip power converters.

ACKNOWLEDGMENTS

The authors gratefully acknowledge the efforts of the staff of the Microelectronics Research Laboratory (MRL) at the IBM T. J. Watson Research Center, where the devices used in this paper were fabricated. This work was supported by the U. S. Department of Energy under Contract No. DE-EE0002892.

¹N. Sturcken *et al.*, International Solid-State Circuits Conference 2012 (to be published).

²N. Sturcken *et al.*, IEEE Custom Integrated Circuits Conference, 2011.

³S. C. O. Mathuna and T. O'Donnell, *IEEE Trans. Power Electron.* **20**, 585 (2005).

⁴D. Gardner *et al.*, *J. Appl. Phys.* **103**, 07E927 (2008).

⁵P. Morrow *et al.*, *IEEE Trans. Magn.* **47**, 2818 (2011).

⁶A. Gromov and V. Korenivski, *IEEE Trans. Magn.* **46**, 2097 (2010).

⁷N. Robertson *et al.*, *IEEE Trans. Magn.* **33**, 2818 (1997).

⁸T. O'Donnell *et al.*, *J. Magn. Magn. Mater.* **322**, 1690 (2010).

⁹S. Roy *et al.*, *J. Magn. Magn. Mater.* **290–291**, 1524 (2005).

¹⁰M. J. Armstrong and N. L. Robertson, IBM Research Report, **10079**, 91895 (1997).

¹¹V. Korenivski *et al.*, *IEEE Trans. Magn.* **32**, 4905 (1996).

¹²E. van de Riet and F. Roozeboom, *J. Appl. Phys.* **81**, 350 (1997).

¹³J. Godsell *et al.*, *J. Appl. Phys.* **107**, 033907 (2010).

¹⁴V. Korenivski and R. B. Van Dover, *J. Appl. Phys.* **82**, 5247 (1997).

¹⁵D. Gardner *et al.*, *IEEE Trans. Magn.* **45**, 4760 (2009).

¹⁶K. D. T. Ngo and M. H. Kuo, Power Electronics Specialists Conference, PESC'88 Record, 19th Annual IEEE, 1988.

¹⁷A. M. Crawford and S. X. Wang, *IEEE Trans. Magn.* **40**, 2017 (2004).